EFFECT OF INTERCRITICAL AUSTENITIZATION AND STARTING MATRIX ON MARTENSITE START TEMPERATURE AND AUSTENITE CARBON CONCENTRATION IN DUCTILE IRON

Harold D. Machado and Ricardo Aristizábal-Sierra
Gipimme, Department of Materials Engineering, Universidad de Antioquia, Calle 67 #53-108, Bloque 18, Oficina 240, Medellín, Colombia

Carlos Garcia-Mateo
Materalia Group, National Center for Metallurgical Research (CENIM-CSIC), Av/ Gregorio del Amo 8, Madrid, Spain

https://doi.org/10.1007/s40962-024-01452-z

Abstract

In this work, the effect of the intercritical austenitization temperature and time, Ni + Cu concentration and starting matrix (fully ferritic or fully pearlitic) on the volume fraction of austenite (fγ), martensite start temperature (Ms) and carbon concentration of the parent austenite (C_0) in ductile iron was investigated using standard metallographic techniques and high-resolution dilatometry. The results showed that a fully pearlitic starting matrix gives higher fγ and C_0 and lower Ms than a fully ferritic starting matrix at the same austenitization temperature under continuous heating. On the other hand, the austenitization time has an effect on the parameters under study only during the first minutes of intercritical austenitization. Finally, at the same intercritical austenitization temperature, the addition of Ni + Cu increases the volume fraction of austenite.

Keywords: *intercritical austenitization, martensite start temperature, parent austenite, ductile iron*

Introduction

Ductile iron is an important engineering material used in the production of parts for the automotive, machinery, mining and agricultural industry, among others.[1] There are specific applications where improved mechanical properties such as better mechanical strength and wear resistance, higher ductility and toughness are needed. One way of improving the mechanical properties of ductile iron is by alloying,[2,3] for example, higher ultimate tensile strength, yield strength and wear resistance can be achieved by alloying with vanadium.[2] Also, a better mechanical response can be achieved by applying heat treatments such as quenching and tempering (Q&T) and low-temperature isothermal transformation (austempering).[4,5]

Different combinations of mechanical properties can be achieved depending on the selected heat treatment route. The Q & T provides high strength, high wear resistance and low ductility and toughness.[4] On the other hand, austempering gives high strength and wear resistance and low to medium ductility and toughness.[5] One way of improving the ductility and toughness of heat-treated ductile iron is by intercritical austenitization, which consists in austenitizing at the intercritical region where ferrite, austenite and graphite coexist. After that, the alloy can be quenched and tempered to obtain a matrix of ferrite plus tempered martensite,[6–9] or austempered to obtain a matrix of ferrite plus ausferrite (bainitic ferrite + high carbon austenite).[1–4,10–14]

There is a fair amount of the literature related to ductile iron submitted on intercritical austenitization. For example, regarding ductile iron with ferrite plus tempered martensite matrices, the available research covers topics such as, the

Received: 24 July 2024 / Accepted: 21 September 2024
Published online: 29 October 2024

influence of tempering[7] and the effect of the martensite volume fraction[6] and its morphology[8] on the mechanical properties and wear resistance.[9] Similarly, the available literature about intercritically austenitized and then austempered ductile iron includes, among others, the influence of the austenitization and austempering temperatures and times on the microstructure and mechanical properties,[4,5,11,12] the effect of Ni and Cu in the lattice elastic constants and mechanical stability of the retained austenite,[15–17] the effect of silicon[18] and thermomechanical processing[19] on the mechanical properties and the machinability of intercritically austempered ductile iron.[20,21]

It is widely reported that in ductile iron austenitized in the intercritical range, as expected, the volume fraction of parent austenite increases, and thus its transformation products (martensite or ausferrite), as the intercritical austenitization temperature raises.[6,11,12] Also, the starting matrix influences the volume fraction, distribution and morphology of the parent austenite during intercritical austenitization.[1,13,22,23] One important aspect of the parent austenite is its chemical composition, which determines among others the martensite start temperature (Ms)[24] and the kinetics of the bainitic transformation.[25–27]

One key element in the transformation of the parent austenite, either to martensite or ausferrite, is carbon. It is well known that carbon concentration of the parent austenite has a large effect on Ms.[28] Also, the carbon concentration of the parent austenite influences the kinetics of the bainitic transformation and the size and relative amount of the transformation products, i.e., a lower carbon concentration in the parent austenite gives a faster bainitic transformation, a coarser microstructure and a higher volume fraction of bainitic ferrite.[25] The available literature indicates that during full austenitization of ductile iron, the carbon concentration of the parent austenite raises with the austenitization temperature.[29] However, the literature on the influence of austenitization parameters, temperature and time, on the carbon concentration of austenite in intercritically austenitized ductile iron is not readily available. This paper examines the formation of austenite and the variation in its carbon concentration during intercritical austenitization of ductile iron with fully ferritic and fully pearlitic starting microstructures.

Experimental Materials and Methods

The alloys for this study were obtained in an induction furnace using 50 kg of ductile iron returns, low carbon steel scrap, low-sulfur graphite and ferrosilicon. Copper and nickel concentrations were adjusted by adding electrolytic copper and 50%Ni-ferronickel. Magnesium treatment (2.0 wt%) and inoculation (0.4 wt%) were performed in an open ladle using a magnesium ferrosilicon alloy (6.5 wt% Mg) and a ferrosilicon-based inoculant (2.7 Ca, 1.5 Al, 2.0 Zr and 0.01 Ce, wt%). Post-inoculation (0.1 wt%) was conducted before pouring into green sand molds to obtain step blocks of 16 mm, 32 mm and 48 mm wall thicknesses. The chemical composition of the alloys was determined by optical emission spectroscopy (OES) in chilled samples using a Bruker Q9 Magellan spectrometer, and carbon was determined using a carbon Leco analyzer (Ref. Leco 523), the results are listed in Table 1. Notice that the variations in chemistry correspond to the concentration of Cu and Ni, while the concentration of additional alloying elements remains similar between the alloys; thus, the experimental results allow understanding also the combined role of Cu and Ni.

Samples for the study were taken from the 16 mm thickness section of the step blocks and prepared using standard metallographic techniques with a final 1 μm diamond polish. A light optical microscope (Nikon, Eclipse MA100 with camera Nikon DS-FI2) was used for graphite characterization in unetched samples according to the ASTM A247 standard.[30] For this purpose, ten fields of view were examined for each alloy using the software ImageJ® with a trap size of 10 μm. Nodularity was 90% for both alloys, and nodule count was around 295 nod/mm^2 for the NiCu alloy and 280 nod/mm^2 for the Base alloy. The as-cast alloys were annealed to get fully ferritic and fully pearlitic matrices as described by Machado et al.[22] which allowed studying the effect of the starting microstructure. Figure 1 shows light optical microscope micrographs of the NiCu alloy, which represent well also the starting microstructures of the Base alloy after annealing. The annealing heat treatments were as follow:

- *Fully ferritic*: Austenitizing at 920 °C for 2 h, then slowly cooled into the furnace at a rate of 1.7 °C/min to 730 °C and isothermally held for 5 h, finally slowly cooled inside the furnace to ambient temperature.

Table 1. Chemical Composition of the Ductile Iron Alloys (wt%)

Alloys	C	Si	Mn	P	S	Cr	Ni	Cu	Mg	CE*
NiCu	3.45	2.70	0.18	0.01	0.007	0.04	0.88	0.60	0.042	4.35
Base	3.53	2.66	0.18	0.01	0.006	0.04	0.12	0.01	0.041	4.42

*Carbon Equivalent: CE=C+1/3Si

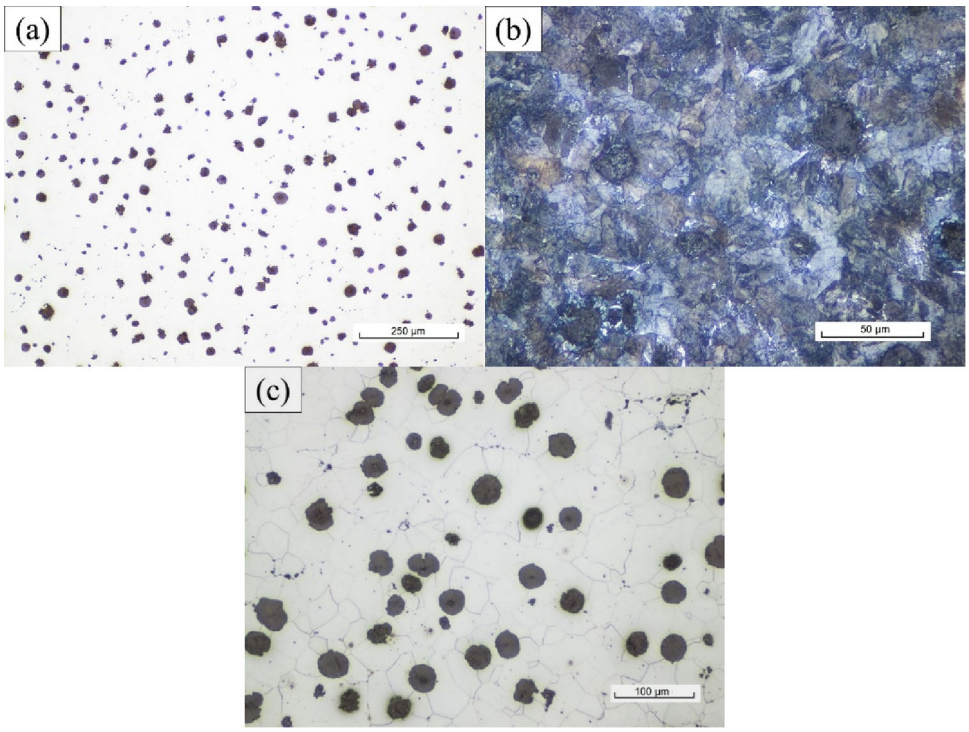

Figure 1. Starting microstructures of the NiCu alloy after annealing: (a) unetched, microphoto taken at 100X, (b) pearlitic sample etched with Nital 2%, microphoto taken at 500X and (c) ferritic sample etched with Nital 2%, microphoto taken at 200X.

Table 2. Austenite Start (TS) and Austenite Finish (TF) Temperatures and Intercritical Range[22,23]

Sample	Alloy	TS, °C	TF, °C	Intercritical range, °C
Pearlitic	NiCu	780	845	65
	Base	784	845	61
Ferritic	NiCu	797	927	130
	Base	792	883	91

- *Fully pearlitic*: Austenitizing at 920 °C for 2 h, then fast cooled to 460 °C and isothermally held for 1 h and then air cooling. The samples were quenched and held into a salt bath (50 wt% KNO3 + 50 wt% $NaNO_2$).

Dilatometric analysis was performed on a Bahr 805A high-resolution dilatometer using cylindrical samples 10 mm in length and 4 mm in diameter. The system consisted of an induction coil, and cooling was applied by blowing helium to the sample, while temperature is controlled by a type K thermocouple welded to the central part of the sample surface. The dilatometry tests were performed using a specific module, equipped with fused silica push-rods to measure the longitudinal changes during different stages of the heat treatments. Preliminary dilatometric tests[22,23] where conducted by heating in vacuum at 0.18 °C/s to 1000 °C in order to determine the austenite start (TS) and finish (TF) temperatures and the intercritical austenitization range. The results are listed in Table 2, they allowed selecting the austenitization temperatures for the dilatometric tests shown in Figure 2 and described as follows:

1. Heating in vacuum at 0.18 °C/s to selected austenitization temperatures:

   a. For ferritic samples: 800, 820, 840, 860, 880 °C and 1000 °C.
   b. For pearlitic samples: 800, 820, 840 °C and 1000 °C.

   Then, the samples were quenched at 100 °C/s with helium to room temperature. After that, Ms was determined according to Sourmail et al.[31] using the 0.2% offset method. This set of experiments was designed to evaluate the effect of the intercritical austenitization temperature under continuous heating on Ms. The highest standard deviation in the determination of Ms using the 0.2% offset method was estimated as 2.5 °C. For this purpose, each full austenitization test was repeated three times.

2. Heating in vacuum at a rate of 0.18 °C/s to selected temperatures within the intercritical austenitization range and holding for 0, 5, 15 and 30 min. The selected intercritical austenitization temperatures were 840 °C and 860 °C for ferritic samples, 820 °C and 840 °C for pearlitic samples of the Base alloy and 790 °C and 820 °C

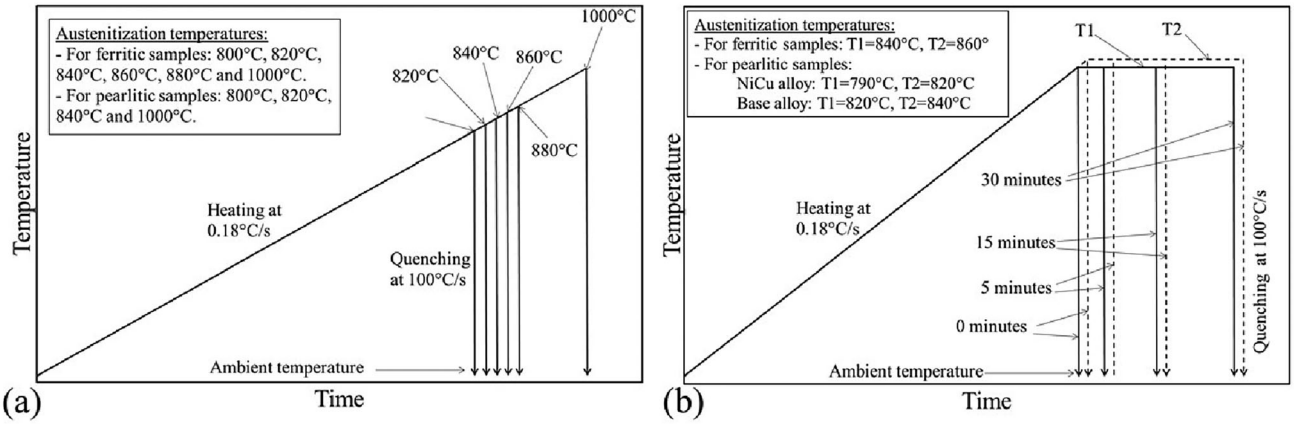

Figure 2. Schematic heat treatment routes for: (a) continuous heating tests and (b) isothermal holding tests.

Table 3. For Both Alloys and Initial Microstructures, Ferritic and Pearlitic, Fraction of Austenite Fγ at Different Austenitization Tγ Under Continuous Heating

Alloy	Sample	Tγ, °C					
		800	820	840	860	880	1000*
Ni-Cu	Ferritic	0.03	0.13	0.43	0.71	0.87	1.00
	Pearlitic	0.67	0.80	0.90	–	–	1.00
Base	Ferritic	0.04	0.06	0.30	0.64	0.75	1.00
	Pearlitic	0.05	0.38	0.64	–	–	1.00

*Fully austenitized

for pearlitic samples of the NiCu alloy. After that, quenching with helium at 100 °C/s. This set of experiments was designed to evaluate the effect of the holding time at the intercritical austenitization temperature on Ms.

The average carbon concentration of the parent austenite (C_0) was calculated using the Ms values collected from the dilatometric tests, the chemical composition in Table 1, in combination with Eqn. 1.[24,32] Notice that this approach does not consider chemical differences within the matrix due to microsegregation.

$$Ms(^{\circ}C) = 520 - 320C - 50Mn - 5Si - 20Ni - 30Cr - 20Mo - 5Cu \quad \text{Eqn. 1}$$

where $C=C_0$

Samples of the experiments just described were prepared using standard metallographic techniques, etched with Nital 2% and analyzed by optical microscopy (Nikon Eclipse MA100 with a Nikon DS-F12 camera) and scanning electron microscopy (SEM, JEOL JSM-6490LV). The volume fraction of martensite in the matrix was determined by systematic point counting according to ASTM E562.[33] The volume fraction of martensite in the matrix was taken as the volume fraction of austenite in the matrix (fγ) at the austenitizing temperature (Tγ), as it has been reported by several researchers in the previous published papers.[1,10–12]

Results and Analysis

Effect of Tγ on fγ Under Continuous Heating

Table 3 lists fγ values determined by point counting at each Tγ for both alloys and starting matrices under study. Notice that as expected, fγ increased as Tγ raised.[6,11,12] Also, the NiCu alloy gives higher fγ at the same Tγ for both starting microstructures, pearlitic and ferritic. Figure 3 shows representative optical micrographs of pearlitic samples after intercritical austenitization under continuous heating followed by quenching. The micrographs in Figure 3 show that at 800 °C under continuous heating, still some undissolved carbides from the pearlite remained in the microstructure of the Base alloy (see Figure 3a), while no carbides were detected in the NiCu alloy (see Figure 3b). Also, both alloys exhibited ferrite from the pearlite dissolution, which appeared preferentially located close and around the graphite nodules because of the higher silicon concentration in this region.[34] Additionally, austenite formation started at the last solidification zones, which is linked to the higher concentration of manganese at these areas.[1,23] At 820 °C, carbides were no longer present in any of the alloys (see Figure 3c, d), and the only phases in the matrix were ferrite and austenite. Finally, at 840 °C (Figure 3e, f), small ferrite islands remained around the graphite nodules, and the matrix was almost fully austenitic in both alloys.

Figure 4 exhibits representative micrographs of ferritic samples of both alloys intercritically austenitized under continuous heating. It can be seen that at 800 °C (Figure 4a, b), austenite started forming at the last solidification zones, then at 840 °C (Figure 4c, d), austenite started

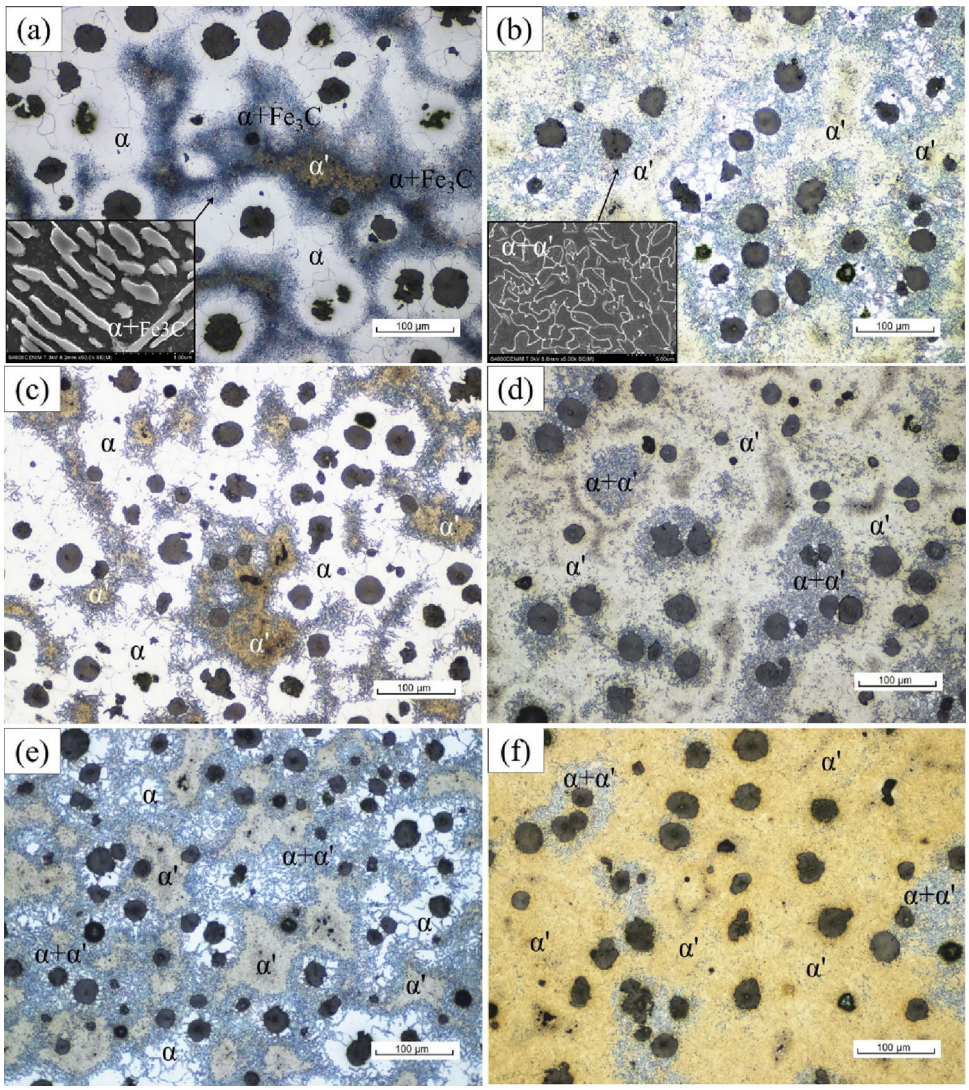

Figure 3. Representative micrographs of pearlitic samples intercritically austenitized under continuous heating. (a) Base alloy at 800 °C, (b) NiCu alloy at 800 °C, (c) Base alloy at 820 °C, (d) NiCu alloy at 820 °C, (e) Base alloy at 840 °C and (f) NiCu alloy at 840 °C. α: ferrite, α': martensite and α+θ: pearlite. Microphotos taken at 200X.

growing from the ferrite grain boundaries toward the interior of the ferrite grains and, finally at 880 °C (Figure 4e, f), the matrix was almost fully austenitic, and only some ferrite at the contours of the graphite nodules remained.

Effect of Tγ on Ms and C_0 Under Continuous Heating

Figure 5 shows representative relative change in length (RCL) vs temperature (T) during cooling of the NiCu and Base alloys with pearlitic and ferritic starting matrices after intercritically austenitization at selected temperatures. The curves in Figure 5 illustrate well the general behavior for the other austenitization temperatures under evaluation. As expected, an increase in the RCL occurred when the face-centered-cubic (FCC) austenite transformed to the body-centered-tetragonal (BCT) martensite, which was linked to the associated unit cell volumetric change.[31] Notice in Figure 5 that the only transformation detected upon cooling was from austenite to martensite, which indicates that the cooling rate was fast enough to avoid the formation of ferrite, pearlite or bainite.

Table 4 and Figure 6 show the results of the determination of Ms and C_0 as a function of Tγ under continuous heating. The data in Figure 6a show that for pearlitic samples, as the austenitization temperature raised within the intercritical range, Ms increased and C_0 decreased. Notice that, within the intercritical range, the Base alloy had a higher C_0 (and as previously mentioned a lower fγ) than the NiCu alloy,

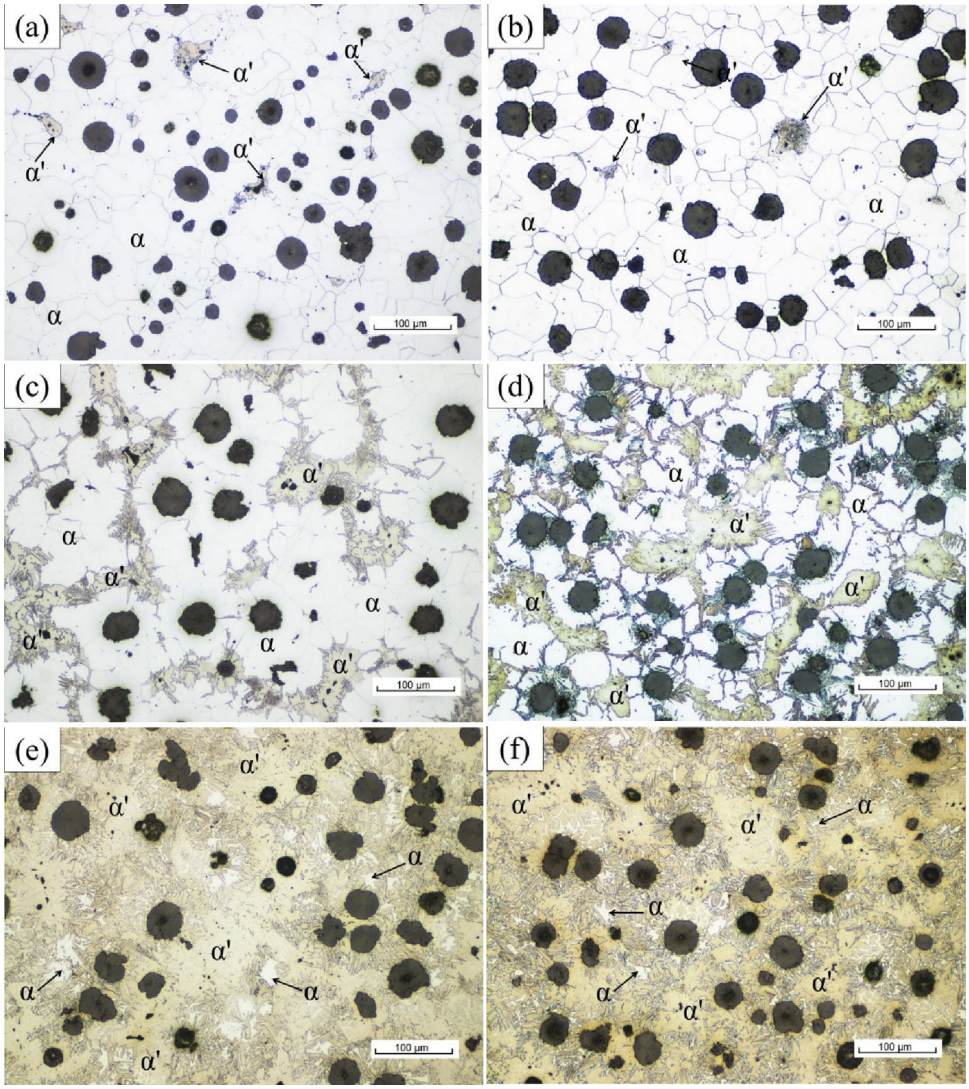

Figure 4. Representative micrographs of ferritic samples intercritically austenitized under continuous heating. (a) Base alloy at 800 °C, (b) NiCu alloy at 800 °C, (c) Base alloy at 840 °C, (d) NiCu alloy at 840 °C, (e) Base alloy at 880 °C and (f) NiCu alloy at 880 °C. α: ferrite and α': martensite. Microphotos taken at 200X.

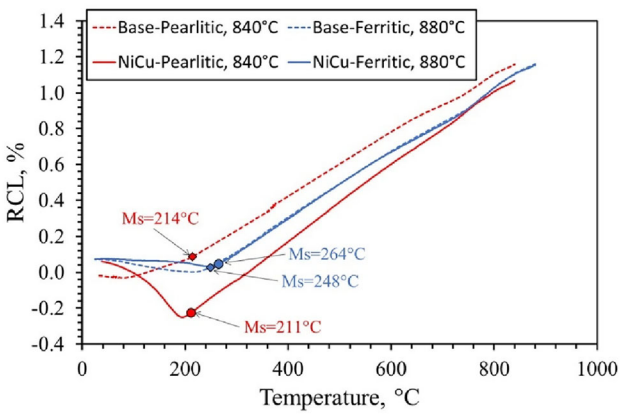

Figure 5. Relative change in length (RCL) versus temperature under cooling of the Base and NiCu alloys: Pearlitic samples intercritically austenitized at 840 °C, and ferritic samples intercritically austenitized at 880 °C.

which suggests that under continuous heating, C_0 in the intercritical range for pearlitic samples depends in the volume fraction of austenite formed, that is, a lower fγ gives a higher C_0.

Table 4 and Figure 6b show Ms and C_0 as a function of Tγ for ferritic samples. At the beginning of the intercritical range, ferritic samples exhibited a similar tendency than pearlitic samples, i.e., Ms increased and C_0 decreased as Tγ raised. However, when Tγ was higher than 840 °C, Ms started decreasing and C_0 began to increase, which indicates an increasing rate of carbon diffusion from the graphite nodules given by the higher austenitization temperature allowing a faster carbon enrichment of the austenite. Again, the results for the ferritic samples show that a higher Tγ gives a higher fγ and a lower C_0. Also, it is worth noticing that pearlitic samples exhibited a higher C_0

Table 4. Martensite Start Temperature (Ms) and Carbon Concentration of the Parent Austenite (C_0) After Austenitization at Different Temperatures (Tγ) Under Continuous Heating

Alloy	Sample	Parameter	Tγ, °C					
			800	820	840	860	880	1000*
NiCu	Ferritic	Ms, °C (±3 °C)	240	253	274	267	264	202
		C_0, wt% (±0.01 wt%)	0.74	0.70	0.65	0.63	0.66	0.86
	Pearlitic	Ms, °C (±3 °C)	188	205	211	–	–	199
		C_0, wt% (±0.01 wt%)	0.90	0.85	0.83	–	–	0.86
Base	Ferritic	Ms, °C (±3 °C)	231	247	261	255	248	211
		C_0, wt% (±0.01 wt%)	0.82	0.77	0.73	0.75	0.77	0.88
	Pearlitic	Ms, °C (±3 °C)	201	210	214	–	–	212
		C_0, wt% (±0.01 wt%)	0.92	0.89	0.88	–	–	0.88

*Fully austenitized

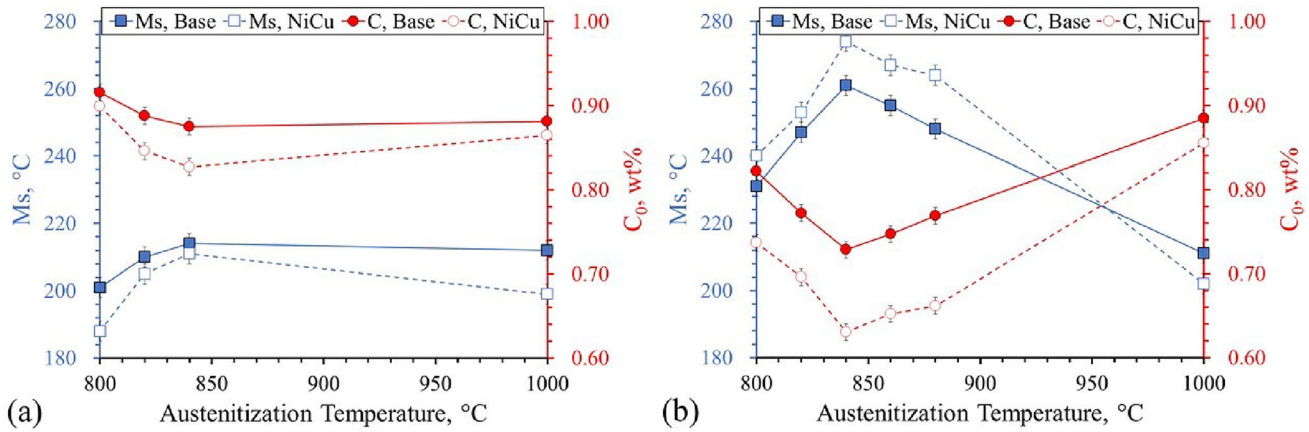

Figure 6. Martensite start (Ms) and carbon concentration of the parent austenite (C_0) as a function of the austenitization temperature under continuous heating: (a) for pearlitic samples and (b) for ferritic samples. Typical deviations are: ±3 °C for Ms and 0.01 wt% for C_0.

than ferritic samples at the same Tγ under continuous heating. Finally, it is relevant to highlight that, when full austenitization is achieved (1000 °C), there is no significant difference in C_0 as a function of the initial microstructure, ferritic or pearlitic.

Effect of tγ on fγ

Figure 7 shows the results of the determination of fγ as function of the austenitization time (tγ) at the intercritical austenitization temperatures selected for all the alloy starting matrices used for this study. The results showed that austenite formation was fast at the beginning of the isothermal holding, decelerated after 5 min of austenitization and nearly did not change between 15 and 30 min. Also, as expected, fγ increases with Tγ for all the alloy starting microstructures under evaluation. Notice that, the pearlitic Base alloy intercritically austenitized at 840 °C gives a higher fγ than the ferritic Base alloy intercritically austenitizaed at the same temperature. Also, the pearlitic NiCu alloy gives a higher fγ at 820 °C than the ferritic NiCu alloy intercritically austenitized at 840 °C, thus the results indicate that a starting pearlitic microstructure gives a higher fγ at the same Tγ than a ferritic starting microstructure.

Figure 8 exhibits optical microscope microphotos of pearlitic samples of the Base alloy intercritically austenitized at different Tγ–tγ. This set of micrographs also represents well the results for the NiCu alloy. The results for pearlitic samples show that austenite formation started at the last solidification zones, also as described before for the continuous heating experiments, ferrite from the pearlite dissolution appeared in the matrix, especially around the graphite nodules where the silicon concentration is higher.[34] After 5 min of isothermal holding, ferritic halos around the graphite nodules were well defined, and some austenite was present at the ferritic grain boundaries close to the graphite nodules. Finally, after 15 min and up to

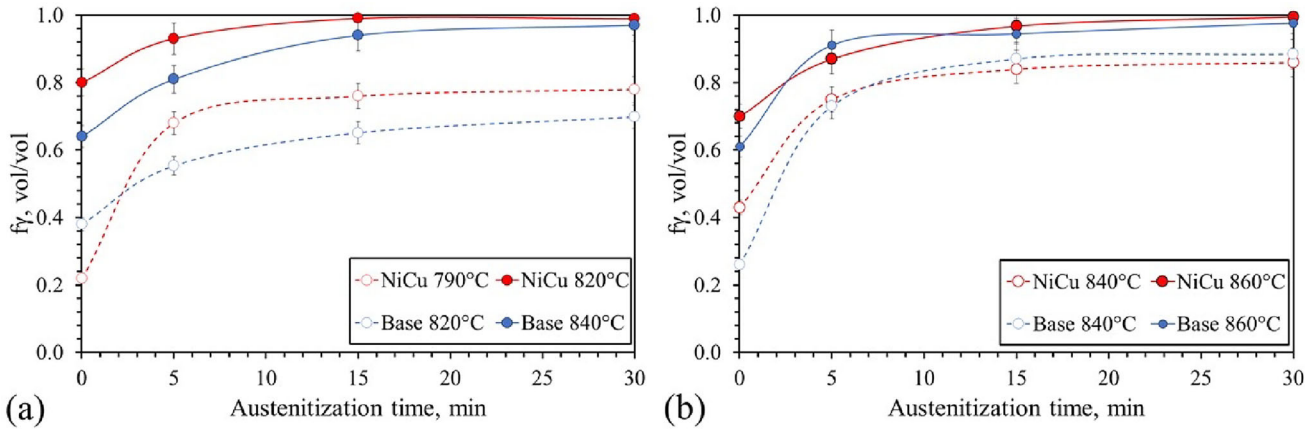

Figure 7. Volume fraction of austenite (fγ) as a function of the autenitization time (tγ) at selected austenitization temperature (Tγ) for: (a) pearlitic samples and (b) ferritic samples.

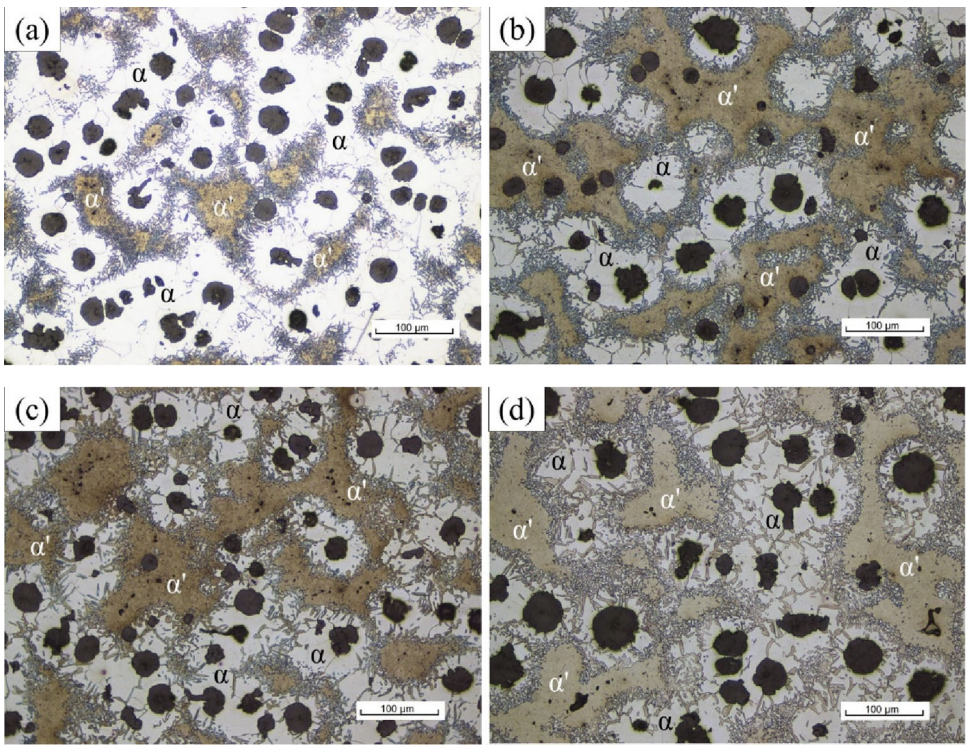

Figure 8. Representative micrographs of pearlitic samples intercritically austenitized at 820 °C for a duration of (a) 0 min, (b) 5 min, (c) 15 min and (d) 30 min. Microphotos taken at 200X.

30 min, the ferrite halos disappeared, and only some small ferritic islands close to the graphite nodules remained in the microstructure.

Regarding ferritic samples, as it can be seen in Figure 9, austenite formation started in the grain boundaries at the last solidification zones. After that, austenite formation continued through the ferritic grain boundaries, and some austenite branches started to connect with the graphite nodules. These austenite branches broadened as the isothermal holding time reached 15 and 30 min.

Effect of tγ on Ms and C_0

Figure 10 displays the results of the determination of Ms and the calculated C_0 for both alloys with pearlitic and ferritic starting microstructures, austenitized at different Tγ within the intercritical range and held for a variety of tγ. The data show that the greatest variations in Ms and C_0 occurred, in both alloys and for ferritic and pearlitic samples, during the first 15 min of isothermal holding, and after that, there was virtually no change.

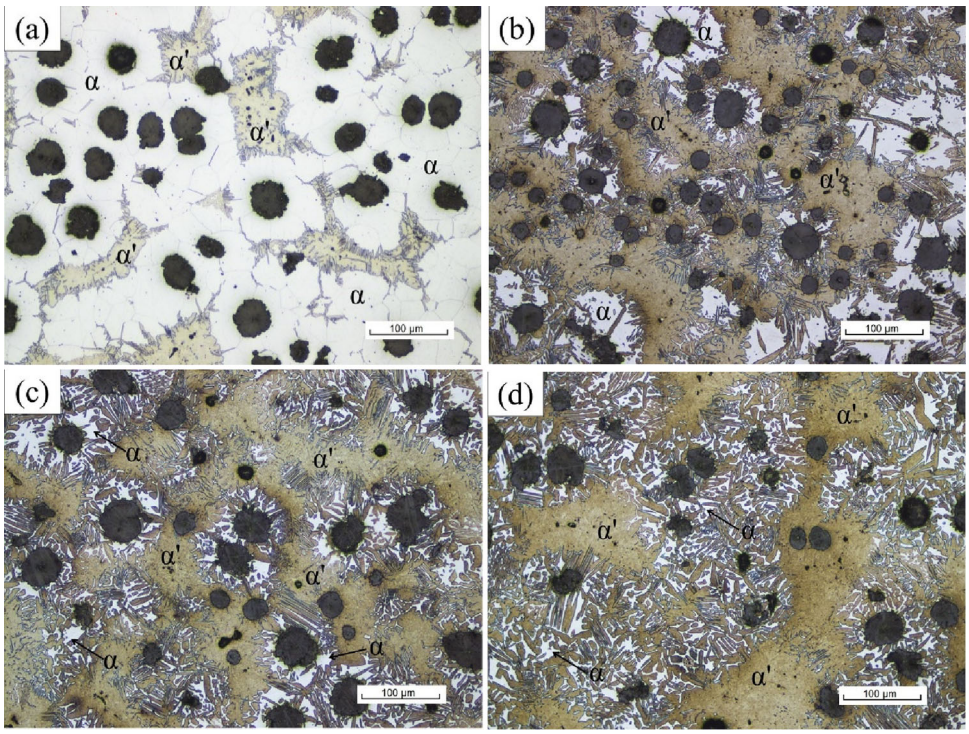

Figure 9. Representative micrographs of ferritic samples intercritically austenitized at 840 °C for a duration of (a) 0 min, (b) 5 min, (c) 15 min and (d) 30 min. Microphotos taken at 200X.

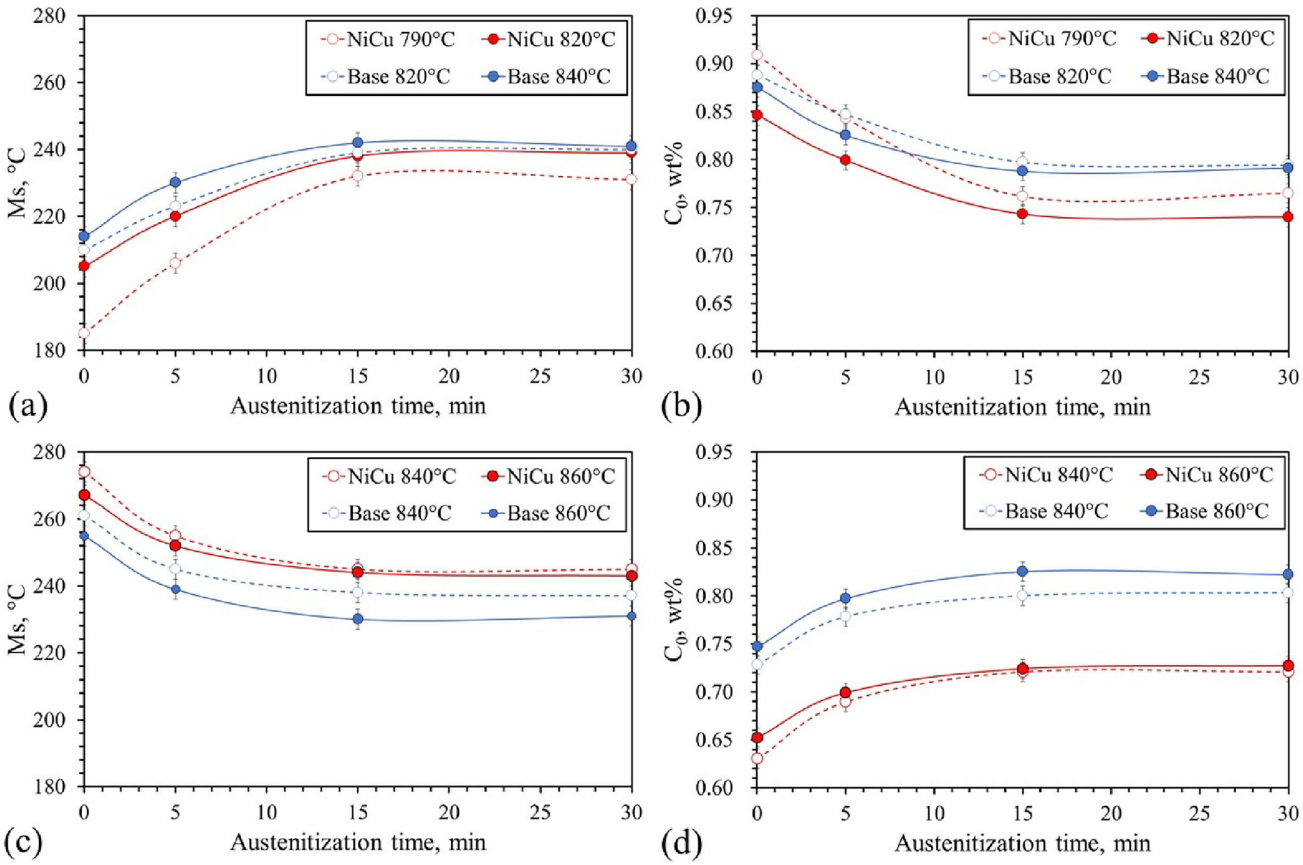

Figure 10. Ms and C_0 as a function of tγ: (a) Ms for pearlitic samples, (b) C_0 for pearlitic samples, (c) Ms for ferritic samples and (d) C_0 for ferritic samples. Typical deviations are: ±3 °C for Ms and 0.01 wt% for C_0.

Figure 10a, b shows that for pearlitic samples Ms raised and C_0 dropped with tγ (up to 15 min). In Figure 10c, d, it can be seen that for ferritic samples, Ms dropped and C_0 raised with tγ (up to 15 min), which is the opposite behavior just described for pearlitic starting microstructures. These results suggest that carbon in solution comes first from pearlite and carbides, then this carbon diffuses creating a higher volume fraction of austenite with a lower carbon concentration, finally carbon diffusion from graphite becomes significant and the concentration of carbon in the austenite and its volume fraction increases simultaneously.

Additionally, for both starting matrixes, the Base alloy exhibited a higher C_0 at the same austenitization temperature, which can be related to its lower fγ given by the differences in the intercritical range. Finally, notice that the results for the Base alloy intercritically austenitized at 840 °C (see Figure 10b, d) indicate that C_0 reaches the same value despite the starting microstructure (pearlitic or ferritic) if the austenitization time is long enough.

Conclusions

The effect of the starting microstructure, ferrite or pearlite, austenitization temperature and time on the formed volume fraction of austenite, martensite start temperature and carbon enrichment of the parent austenite were investigated for ductile iron during intercritical austenitization. The results showed that:

1. The austenite volume fraction (fγ) depends mostly on Tγ and the starting microstructure, a higher Tγ and a pearlitic starting microstructure gives higher fγ. Regarding tγ, it has a significant influence at the initial stages of austenitization, but after 15 min, it does not seem to have an important effect on fγ.
2. The effect of tγ in Ms and C_0 depends on the starting microstructure, when the starting microstructure is pearlitic Ms increases and C_0 dropped up to 15 min of intercritical austenitization, ferritic starting microstructure exhibited an opposite behavior. However, after 15 min and up to 30 min of intercritical austenitization, Ms and C_0 did not change significantly and reach similar values regardless of the initial microstructure.
3. The effect of Tγ on Ms and C_0 also depends on the initial microstructure, if the initial microstructure is pearlitic a higher Tγ gives a higher Ms and a lower C_0, while ferritic initial microstructures gives the opposite behavior.

Funding

Open Access funding provided by Colombia Consortium.

REFERENCES

1. W.L. Guesser, C.L. Lopes, P.A.N. Bernardini, Austempered ductile iron with dual microstructures: effect of initial microstructure on the austenitizing process. Inter Metalcast **14**, 717–727 (2020). https://doi.org/10.1007/s40962-019-00397-y
2. A.S. Kandemir, R. Gecu, Influence of vanadium content and cooling rate on the characteristics of vanadium-alloyed spheroidal graphite cast irons. J. Alloy. Compd. (2023). https://doi.org/10.1016/j.jallcom.2022.168017
3. A. Sandikoglu, R. Gecu, Microstructural, mechanical and tribological characterization of aluminum-alloyed ductile cast irons based on aluminum content. J. Alloy. Compd. **879**, 160428 (2021). https://doi.org/10.1016/j.jallcom.2021.160428
4. A. Uyar, O. Sahin, B. Nalcaci et al., Effect of austempering times on the microstructures and mechanical properties of dual-matrix structure austempered ductile iron (DMS-ADI). Inter Metalcast **16**, 407–418 (2022). https://doi.org/10.1007/s40962-021-00617-4
5. P. Sellamuthu, D.G.H. Samuel, D. Dinakaran, V.P. Premkumar, Z. Li, S. Seetharaman, Austempered ductile iron (ADI): influence of austempering temperature on microstructure, mechanical and wear properties and energy consumption. Metals. **8**(1), 53 (2018). https://doi.org/10.3390/met8010053
6. R. Aristizabal, R. Foley, A. Druschitz, Intercritically austenitized quenched and tempered ductile iron. Inter Metalcast **6**, 7–14 (2012). https://doi.org/10.1007/BF03355534
7. M. Rashidi, M. Moshrefi-Torbati, Effect of tempering conditions on the mechanical properties of ductile cast iron with dual matrix structure (DMS). Mater. Lett. **45**(3), 203–207 (2000). https://doi.org/10.1016/S0167-577X(00)00105-1
8. K. Kocatepe, M. Cerah, M. Erdogan, Effect of martensite volume fraction and its morphology on

the tensile properties of ferritic ductile iron with dual matrix structures. J. Mater. Process. Technol. **178**(1–3), 44–51 (2006). https://doi.org/10.1016/j.jmatprotec.2005.11.019
9. Y. Sahin, M. Erdogan, M. Cerah, Effect of martensite volume fraction and tempering time on abrasive wear of ferritic ductile iron with dual matrix. Wear **265**(1–2), 196–202 (2008). https://doi.org/10.1016/j.wear.2007.10.004
10. E. Druschitz, M. Ostrander, R. Aristizabal, The science of intercritically austempered ductile iron (IADI). AFS Trans **119**, 19–21 (2014)
11. A.D. Basso, R.A. Martínez, J.A. Sikora, Influence of austenitising and austempering temperatures on microstructure and properties of dual phase ADI. Mater. Sci. Technol. **23**(11), 1321–1326 (2007). https://doi.org/10.1179/174328407X236544
12. M. Erdogan, V. Kilicli, B. Demir, Transformation characteristics of ductile iron austempered from intercritical austenitizing temperature ranges. J. Mater. Sci. **44**(5), 1394–1403 (2009). https://doi.org/10.1007/s10853-006-1415-7
13. L. Lopes, *"Estudo da Influência da Microestrutura na Cinética de Austenitização na Zona Crítica e Propriedades Mecânicas de Ferros Nodulares Austemperados Duais" Tese* (Universidade Federal De Santa Catarina, Florianópolis, 2014)
14. M. Pellizzari et al., Trattamenti termici austempering kinetics of a ductile iron Memorie. La Metallurgia Italiana n **10**, 15–20 (2015)
15. R.E. Aristizabal, A.P. Druschitz, E. Druschitz, R. Bragg et al., Intercritically austempered ductile iron. AFS Trans. **119**, 407–412 (2011)
16. A.P. Druschitz, R.E. Aristizabal, E. Druschitz et al., In situ studies of intercritically austempered ductile iron using neutron diffraction. Metall. Mater. Trans. A **43**, 1468–1476 (2012). https://doi.org/10.1007/s11661-011-0921-7
17. A. Druschitz et al., Neutron diffraction studies of intercritically austempered ductile irons. SAE Int. J. Mater. Manuf. **4**(1), 111–18 (2011)
18. N.E. Tenaglia et al., Influence of silicon content on mechanical properties of IADI obtained from as cast microstructures. Int. J. Cast Met. Res. **33**(2–3), 72–79 (2020). https://doi.org/10.1080/13640461.2020.1756082
19. M. Soliman, H. Palkowski, Effect of thermo-mechanical processing on structure and properties of dual-phase matrix ADI with different Si-contents. Int. J. Met. **14**(3), 853–860 (2020). https://doi.org/10.1007/s40962-020-00477-4
20. A.P. Druschitz, D. Fitzgerald, *"MADITM: Introducing a new, machinable austempered ductile iron", SAE technical paper 2003–01-0187* (Society of Automotive Engineers, Warrendale, 2003)
21. M. Sabzalipour, A.M. Rashidi, Machinability of martensitic and austempered ductile irons with dual matrix structure. J. Market. Res. **26**, 6928–6941 (2023). https://doi.org/10.1016/j.jmrt.2023.09.054
22. H.D. Machado, R. Aristizabal-Sierra, C. Garcia-Mateo, I. Toda-Caraballo, Effect of the starting microstructure in the formation of austenite at the intercritical range in ductile iron alloyed with nickel and copper. Int. J. Met. **14**(3), 836–845 (2020). https://doi.org/10.1007/s40962-020-00450-1
23. H.D. Machado, I. Toda-Caraballo, C. Garcia-Mateo, R. Aristizábal-Sierra, Modelling the formation of austenite in the intercritical interval in ductile iron. J. Market. Res. **16**, 1445–1457 (2022). https://doi.org/10.1016/j.jmrt.2021.12.072
24. S.-J. Lee, M. Jung, Prediction of martensite start temperatures of highly alloyed steels. Arch. Metall. Mater. **66**(1), 107–111 (2021). https://doi.org/10.24425/amm.2021.134765
25. H.K.D.H. Bhadeshia, *Bainite in steels* (IOM Communications Ltd, London, 2001)
26. U. Batra, S. Ray, S.R. Prabhakar, The Influence of nickel and copper on the austempering of ductile iron. J. Mater. Eng. Perform. **13**(1), 64–68 (2004). https://doi.org/10.1361/10599490417515
27. E. Tyrała, H. Lopez, Effect of copper and nickel on the transformation kinetics of austempered ductile iron. J. Mater. Eng. Perform **23**(October), 3505–3510 (2014). https://doi.org/10.1007/s11665-014-1167-5
28. G. Krauss, 12.11 - Quench and tempered martensitic steels: microstructures and performance, in *Comprehensive Materials Processing*, ed. by S. Hashmi, G.F. Batalha, C.J. Van Tyne, B. Yilbas (Elsevier, 2014), pp. 363–378. https://doi.org/10.1016/B978-0-08-096532-1.01212-7
29. M. Grech, J.M. Young, Effect of austenitising temperature on tensile properties of Cu–Ni austempered ductile iron. Mater. Sci. Technol. **6**(5), 415–421 (1990). https://doi.org/10.1179/mst.1990.6.5.415
30. ASTM standard A247 - 16a, (2016) "Standard Test Method for Evaluating the Microstructure of Graphite in Iron Castings," a247, 67(Reapproved):1–13
31. T. Sourmail, V. Smanio, Determination of Ms temperature: methods, meaning and influence of 'slow start' phenomenon. Mater. Sci. Technol. (United Kingdom) **29**(7), 883–888 (2013). https://doi.org/10.1179/1743284713Y.0000000209
32. G.E. Totten, M.A.H. Howes, *Steel Heat Treatment Handbook* (Marcel Dekker, New York, 1997)
33. ASTM E562, (2011) "Standard test method for determining volume fraction by systematic manual point count," Practice, no. C, pp. 1–7
34. T. Kobayashi, H. Yamamoto, Development of high toughness in austempered type ductile cast iron and evaluation of its properties. Met. Trans. A **19**, 319–327 (1988). https://doi.org/10.1007/BF02652541